Liquid Phase Heteroepitaxial Growth of Moisture-Tolerant MOF-5 Isotype Thin Films and Assessment of the Sorption Properties by Quartz Crystal Microbalance

*Suttipong Wannapaiboon, Min Tu, and Roland A. Fischer**

The moisture-tolerant metal-organic frameworks (MOFs) of formula $[Zn_4O(L)_3]_n$ (L = di-substituted carboxypyrazolate derivatives) are fabricated as thin films on self-assembled monolayer (SAM) functionalized gold substrates by employing the step-by-step liquid phase epitaxial (LPE) deposition method in a continuous operation mode. The in situ monitoring of the deposition by quartz crystal microbalance (QCM) and grazing incidence X-ray diffraction reveal different growth regimes and crystallinities of the obtained thin films in dependence of the chosen alkyl side chain functionality at the carboxypyrazolate linkers, L. To overcome the relatively poor crystallinity and low porosity of a particular homostructured metal-organic framework type B film, the step-by-step heteroepitaxial growth of this MOF B on top of the crystallite surfaces of a well-grown and lattice-matched MOF type A is applied. This approach enables the fabrication of oriented, core-shell-like MOF B@A surface mounted heterocrystals as an intergrown homogeneous coating for the selective adsorption of volatile organic compounds. The accessible pore volumes of the individual components and the heterostructured films are characterized by performing adsorption measurements of different organic probe molecules using an environmentally controlled QCM instrument. The results show good adsorption capacity, excellent size exclusion selectivity for alcohols, and a high degree of moisture-tolerance of the heteroepitaxial MOF films.

1. Introduction

Metal-organic frameworks (MOFs; also called porous coordination polymers, PCPs)[1] have attracted much attention as fascinating prospects for gas storage,[2] gas separation,[3] catalysis,[4] sensing,[5] and medical applications.[6] One outstanding feature of this class of high-performance porous materials is the possibility for rational synthesis. The framework topologies can be designed by selecting metal ion clusters as nodes and appropriate organic linkers to connect these building blocks. The properties of the MOFs depend not only on chemical functionality but also on the pore structure, size and shape. To achieve the targeted performances of MOFs, the force fields and coordination space within the pores, as well as the reactive centers of the framework, need to be optimized.[7] However, the direct introduction of more sophisticated chemical functionalization under solvothermal synthetic conditions is limited, and certain substituents at the linkers may prevent the formation of the desired MOFs as a result of interference with the desired coordination chemistry of the metal ion nodes. Post-synthetic modification (PSM) circumvents this problem by interchanging organic functional groups at the linkers after the construction of the parent MOF.[8] Another effective methodology for MOF functionalization is the homoepitaxial and heteroepitaxial growth of some MOF **B** on the surface of a chosen MOF **A** seed crystal. This method provides a heterostructured core-shell type material, **B@A**, that both conserves the characteristic features of MOF **B** and **A** and shows hybrid properties as a functional unit.[9] Based on the lattice matching between MOFs **A** and **B** and the seeding concept, heterometallic core-shell $[M_2L_2P]_n$ MOF crystals ($M = Zn^{2+}$ and Cu^{2+}, L = anionic dicarboxylate layer linkers and P = neutral bidentate nitrogen pillar linkers), as well as core-shell IRMOF crystals $[Zn_4OL'_3]_n$ with different L′ dicarboxylate linkers, were successfully synthesized.[9a,b] Moreover, the heteroepitaxial growth of $[M_2L_2P]_n$ MOFs using two different bidentate nitrogen pillar linkers (P) results in the face-selective formation of hybrid **BAB**-type MOF crystals, of which the second crystals, **B**, can be fabricated only along the *c*-axis or the (001) facets of the seed crystals, **A**. This result emphasizes the need for matching both the coordination chemistry and the lattice parameters between the different components in the solvothermal epitaxial growth of such free standing hybrid MOF crystals.[9c] Accordingly, multifunctional MOF materials are emerging, and these materials provide integrated properties through the design of micro-scale derivatives (e.g., functionalized linkers, fu-Ls) and the meso-scale arrangement of the different sub-unit crystals. The key idea to achieving the desired features is the controlled arrangement of each individual component with a specific functionality at the desired spatial positions within the materials.[9d–f] For example, the variation of

S. Wannapaiboon, M. Tu, Prof. R. A. Fischer
Chair of Inorganic Chemistry II-Organometallics
and Materials Chemistry Ruhr-Universität Bochum
D-44780, Bochum, Germany
E-mail: roland.fischer@rub.de

DOI: 10.1002/adfm.201302854

the size of the organic linkers in the core-shell based $[M_2L_2P]_n$ material leads to size-selective separation (molecular sieve) at the shell crystal (smaller pore window) and to the preservation of a high-capacity storage container at the core crystal (larger pore opening and volume).[9d] Furthermore, the combination of PSM together with epitaxial growth leads to the specific functionalization only at the reactive groups within the shell components. As a result, the structurally modified hybrid core-shell MOF crystal provides a selective adsorption of one type of guest molecules with different chemical functionalities over the others.[9e]

The integration of functionalized MOF materials in microsystems and devices requires the deposition of MOF thin films onto given substrates. Thus far, the reported results on this topic indicate potential for various applications,[10] such as chemical sensors,[11] separating membranes[12] and capillary columns for gas chromatography.[13] Most concepts of the bulk MOF synthesis of both single-component and hybrid crystals are transferable to MOF thin film processing. The step-by-step liquid phase epitaxial growth method (LPE) is one superior method[10b] to achieve well-defined layer thickness or crystallite sizes, even down to the scale of one elementary cell, together with precisely controlled crystallographic orientation. In the ideal case of strictly self-terminated growth kinetics, this method leads to the so-called surface mounted metal-organic framework thin films (SURMOFs).[14] Using the controlled SBU approach (CSA), the step-by-step LPE method allows the growth of SURMOFs at relatively low temperature via the sequential contact of the chosen substrates with solutions of the selected inorganic and organic building blocks.[15] In particular, various heterostructured SURMOFs of $[M_2L_2P]_n$ were obtained by LPE on self-assembled organic monolayer (SAM) modified gold substrates and have been thoroughly examined.[16] Unlike bulk crystals, the location and distribution of functionalities in the coatings can be designed based on the sequence and number of deposition cycles of each component. Moreover, the in situ monitoring of LPE growth by using surface plasmon resonance (SPR) spectroscopy,[16a] or a quartz crystal microbalance (QCM) instrument,[16b,c,17] allows for direct process control and provides insight into the deposition mechanism.

For practical applications of MOFs, including thin films and membranes, chemical, thermal and mechanical stability are required. Moreover, the materials must maintain their good adsorptive, selective and separating performances even when operated at ambient conditions. Recently, Montoro et al. reported the robust MOF of formula $[Zn_4O(dmcapz)_3]_n$ (dmcapz = 3,5-dimethyl-4-carboxypyrazolato),[18] which features the desired properties and is in contrast to the very moisture-labile and closely structurally related $[Zn_4O(bdc)_3]$ (called IRMOF-1 or MOF-5; bdc = 1,4-benzenedicarboxylate). In our previous communication, we fabricated thin films of $[Zn_4O(dmcapz)_3]_n$ at a relatively low temperature of 50 °C in an ethanol/water solvent system and investigated the adsorption properties using an environmentally controlled QCM.[19] However, our previously applied stepwise deposition was performed in a static mode, that is, through the batchwise immersion of the substrate into the precursor and washing solutions. This non-continuous conduction of the LPE was found to be of limited versatility because it was difficult or even impossible to achieve highly crystalline films of some $[Zn_4O(L)_3]_n$, with L being functionalized derivatives of the dmcapz parent linker.

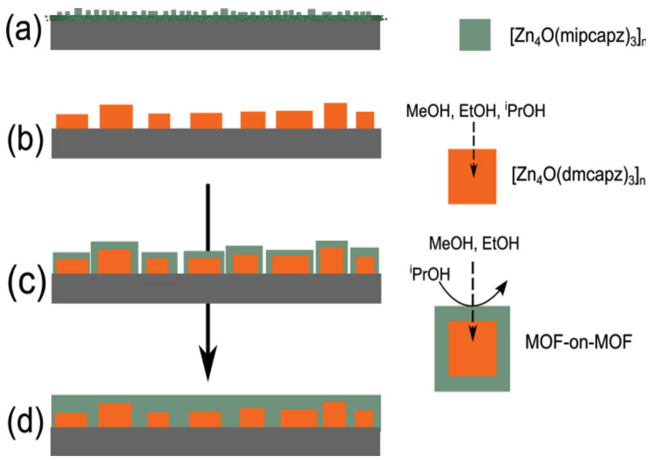

Scheme 1. The illustration of the $[Zn_4O(L)_3]_n$ film growths by the continuous step-by-step LPE deposition indicates a) the moderately crystalline homostructured $[Zn_4O(mipcapz)_3]_n$ film after 40 deposition cycles, b) the highly crystalline $[Zn_4O(dmcapz)_3]_n$ after 20 deposition cycles acting as the core component, c) the early stage of a heteroepitaxial growth of the $[Zn_4O(mipcapz)_3]_n$ shell component on top of the $[Zn_4O(dmcapz)_3]_n$ core, and d) the fully covered heteroepitaxial MOF-on-MOF films showing high crystallinity and selective adsorption of methanol and ethanol over isopropanol molecules based on the size selection by the pore opening window of the shell component.

Herein, we report significant improvement of the quality of such homostructured, functionalized films and the fabrication of related heterostructured MOF films **B@A** using the continuous, automated step-by-step LPE process monitored by QCM. By taking advantage of LPE growth, a suitably selected MOF film **A** is fabricated as seeds to achieve a perfect crystallinity of MOF **B** as a shell-type coating on top of the pre-deposited core-type crystals, **A** (**Scheme 1**). Size-selective adsorption, moisture-tolerant capability and possibilities for using these heterostructured MOF films in separating applications are discussed in detail below.

2. Results and Discussion

Continuous step-by-step LPE was applied to fabricate thin films of $[Zn_4O(L)_3]_n$. We would first like to note that the applied experimental protocol is characterized by the alternate dosing of solutions of the separated MOF building blocks onto a given substrate in a continuous flow with very small dead volume, which is in contrast to a static (batchwise) step-by-step LPE.[19] The applied growth technique, however, does not imply that the actual film growth kinetics will or should follow a strictly self-terminated layer-by-layer growth mechanism. To avoid any confusion, we do not use the acronym SURMOFs for the MOF thin films discussed in this study and suggest using the definition SURMOF only for those MOF thin films for which the growth mode matches a self-limited mechanism.

MOF film growths were checked on two differently functionalized QCM substrates that had either a –COOH or –OH terminated SAM surface (Figures S1,S2; Supporting Information; SAM = self-assembled organic monolayer). According to the out-of-plane XRD patterns, thin films of $[Zn_4O(dmcapz)_3]_n$ were obtained as a pure phase with high crystallinity on both types of functionalized substrates after 20 deposition cycles at 40 °C. However, a slightly higher degree of crystallinity (i.e., relative XRD peak intensity) was observed on the –COOH surface. Preferred crystallite orientation along the [100] direction was observed, which corresponds to the preferable attachment of the cubic MOF crystallites to the substrate surface by their bottom facet.[19] The film porosity was evaluated by methanol adsorption. The Langmuir type I isotherms at 25 °C of both films emphasize similar adsorption properties with a specific methanol adsorption amount at a saturation level of approximately 7.3 mmol g^{-1}. Scanning electron microscopic (SEM) images of the films (Figure S2, Supporting Information) suggest some advantages of using the –COOH terminated surfaces as substrates for this study. The better surface coverage indicates a more efficient nucleation compared with the –OH terminated surface. This occurrence may be explained by the better compatibility of the –COOH functional groups of the SAM functionalized surface with the employed component $[Zn_4O(CH_3COO)_6]$ for the CSA (controlled SBU approach), which is of particular relevance for nucleation during the first deposition cycles. Therefore, the –COOH functionalized QCM substrates were selected for further studies.

2.1. Homostructured $[Zn_4O(L)_3]_n$ MOF Films: Growth and Adsorption Properties

2.1.1. MOF Film Growth

The pore size of $[Zn_4O(L)_3]_n$ can be varied by the substitution in the 3,5-position at the carboxylpyrazolato (capz) components, L. One possibility is the substitution of the methyl groups on dmcapz with other alkyl groups. The unit cell parameters of the synthesized $[Zn_4O(L)_3]_n$ MOFs will either remain unchanged or deviate slightly.[19] According to the XRD patterns of the obtained MOF films (**Figure 1**), the continuous step-by-step LPE method affords crystalline, homostructured $[Zn_4O(L)_3]_n$ films upon the appropriate selection of the linker, L. Excellent crystallinity of these samples (Figures 1b–d), as qualitatively judged by the very high signal-to-noise ratio of the XRD patterns, could be achieved for H_2L, such as 3,5-dimethyl-4-carboxypyrazole (H_2dmcapz), 3-methyl-5-ethyl-4-carboxypyrazole (H_2mecapz) and 3-methyl-5-propyl-4-carboxypyrazole (H_2mpcapz), whereas a moderate signal-to-noise ratio (Figure 1e) was observed for 3-methyl-5-isopropyl-4-carboxypyrazole (H_2mipcapz). Interestingly, the more bulky alkyl substituents of 3-methyl-5-butyl-4-carboxypyrazole (H_2mbcapz) and 3,5-dipropyl-4-carboxypyrazole (H_2dpcapz) disfavored the formation of the cubic MOF-5 isotype phase under the conditions of the growth experiment. Instead of the expected $[Zn_4O(L)_3]_n$ phase, a different crystalline phase was observed, and it appeared to exhibit a so far unknown structure (Figures 1f, 1g). Obviously, there is a limitation for pore size modification when fabricating this carboxypyrazolate $[Zn_4O(L)_3]_n$ MOF as a thin film at moderate temperatures.

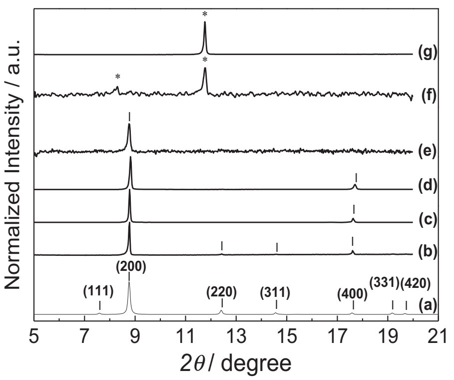

Figure 1. a) Simulated XRD pattern of cubic MOF-5 isotype $[Zn_4O(dmcapz)_3]_n$ powder according to the published data[17] (indicated by the | symbol). XRD patterns of the thin films of b) $[Zn_4O(dmcapz)_3]_n$, c) $[Zn_4O(mecapz)_3]_n$, d) $[Zn_4O(mpcapz)_3]_n$, and e) $[Zn_4O(mipcapz)_3]_n$ fabricated by the continuous step-by-step LPE deposition at 40 °C for 40 cycles [each cycle consists of continuous flow of the solution of basic zinc acetate 10 min/ethanol 5 min/linker 10 min/ethanol 5 min] on the –COOH functionalized QCM substrates and the unknown phase (indicated by the * symbol) obtained when using f) H_2mbcapz and g) H_2dpcapz as the linker.

The growth was monitored in situ using the changing QCM frequency as a function of deposition time (corresponding to number of deposition cycles). The frequency change is proportional to the mass change, according to the Sauerbrey equation, when the films are thin, rigid and tightly bound to the substrate surface.[17,20] The similarity of frequency changes in different harmonics and the overall small dissipation after the completion of each deposition cycle were observed in our experiments (Figure S3, Supporting Information). These data support the applicability of the Sauerbrey equation. While it would be interesting to obtain a closer inspection of the QCM frequency change and dissipation effects, as one referee requested, our study is not directed at investigating the particular growth kinetics and elucidating the growth mechanism in great detail. Instead, our focus is the functionality of the targeted heterostructured MOF **B@A** films.

The overall mass uptakes were determined to be a linear function of the number of deposition cycles, which allows for the precise control of the film growth using the employed method. Unlike the continuous LPE deposition of SURMOFs, for example, HKUST-1[17] and $[M_2L_2P]_n$ MOFs,[15,16,21] the mass uptake of $[Zn_4O(L)_3]_n$ (e.g., $[Zn_4O(dmcapz)_3]_n$ in Figure S4, Supporting Information) increases with each deposition step of the zinc component without pronounced saturation, indicating no self-termination (at least under the chosen conditions). However, the frequency becomes stable after performing the washing step, which relates to the permanent chemisorption of the zinc components to the surface (showing small dissipation). In each subsequent deposition step of the H_2L linker solutions, the mass uptake increases until reaching saturation, after which it decreases and stabilizes during the ethanol washing step. The highly increasing dissipation during the beginning of linker deposition indicates that the linkers are not initially attached in a rigid fashion to the surface. Eventually, substitution of the remaining acetate groups in the previously surface

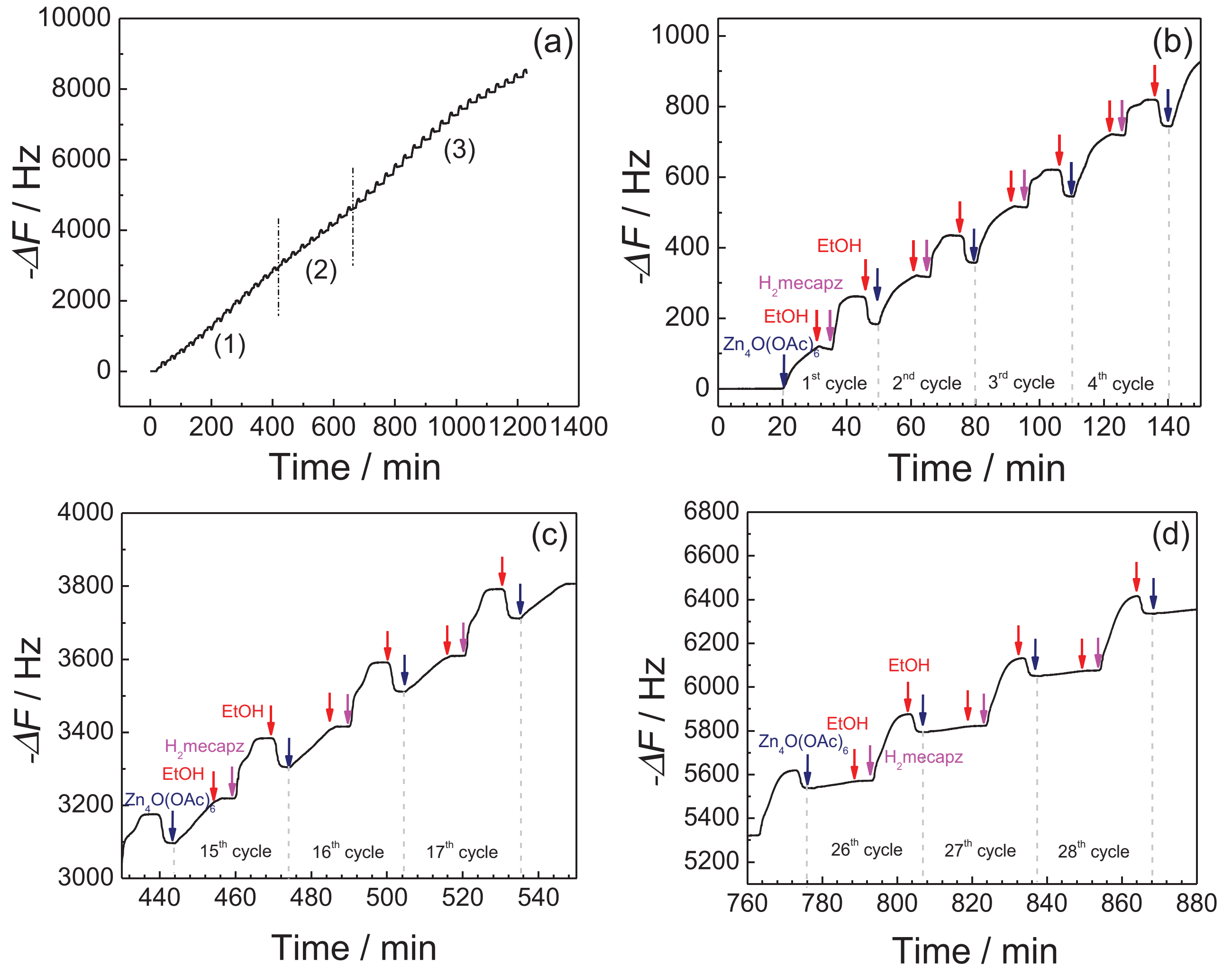

Figure 2. a) In situ monitoring of the QCM frequency as a function of deposition time during the continuous step-by-step growth of $[Zn_4O(mecapz)_3]_n$ film at 40 °C for 40 cycles. QCM profiles representing the different sections of film growth as depicted in b) section (1), c) section (2), and d) section (3) in (a).

chemisorbed $[Zn_4O(CH_3COO)_6]$ components occurs, and the excess linkers and substituted acetate units are removed during the following washing step (finally showing small dissipation). Clearly, the $[Zn_4O(L)_3]_n$ films obtained by the continuous step-by-step LPE method are not grown via a self-terminated "layer-by-layer" growth mechanism, as found for HKUST-1 (which is the only rigorously investigated case). Instead, an island growth mode in the nucleation stage and the subsequent overgrowth of the pre-formed MOF crystallites on all facets in a core-shell fashion occurs.

The frequency change curves during the film formation of $[Zn_4O(mecapz)_3]_n$ (**Figure 2**) and $[Zn_4O(mpcapz)_3]_n$ (Figure S5, Supporting Information) show three distinct sections with different growth behaviors. During the first few cycles, the growth behavior is similar to the growth of $[Zn_4O(dmcapz)_3]_n$. With increasing number of deposition cycles, the final mass uptake during the deposition of the linker is higher, whereas the uptake of basic zinc acetate becomes lower, until showing a tiny uptake at the final section of deposition. This observation may be explained in the following way. The uptake of basic zinc acetate plays an important role in the early stage of deposition and is relevant for the control of nucleation and, thus, the formation of the desired MOF phase at the functionalized surface. The alteration of the growth mode during the last stage indicates the transition from the nucleation and early crystallite growth stage to the steady-state crystal growth stage, which requires a relatively higher mass uptake of the linker. As a result of this growth scheme, the obtained MOF films show excellent morphology and crystallinity (**Figure 3**).

Moreover, the two-dimensional grazing incidence X-ray diffraction (2D-GIXRD) patterns of $[Zn_4O(mecapz)_3]_n$ and $[Zn_4O(mpcapz)_3]_n$ show discrete patterns that indicate the highly preferred orientations of the crystal planes. The out-of-plane cuts from the 2D-GIXRD patterns at the azimuth angle of 0°, corresponding to the lattice planes parallel to the substrate surface, show only the diffraction peaks relating to the [100] orientation with very high intensities. Interestingly, the other lattice planes, that is, (111), (220), and (311), become significant

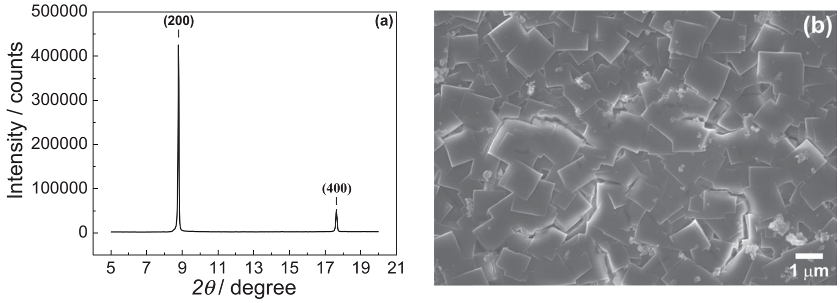

Figure 3. a) The XRD pattern (Bragg-Brentano geometry, exposure time 30 min) and b) the SEM image of the $[Zn_4O(mecapz)_3]_n$ MOF films obtained from the continuous step-by-step LPE deposition at 40 °C for 40 cycles indicate a very high crystallinity with preferred orientation along the [100] direction (attaching the bottom facet of the cubic particles to the substrate surface).

only in the oblique directions with respect to the substrate surface (Figures S7,S8, Supporting Information). The 2D-GIXRD data and the SEM images (Figure 3 and Figure S9) provide evidence of well-oriented, highly crystalline MOF films. The cubic crystallites attach by the bottom (100) facet to the –COOH terminated substrate surface in the nucleation stage, with the further crystallite growth occurring homoepitaxially along the facets corresponding to the [100] direction of the methyl/ethyl-substituted $[Zn_4O(mecapz)_3]_n$ and the methyl/propyl-substituted $[Zn_4O(mpcapz)_3]_n$ MOFs. The typical film thickness was approximately 1 μm after 40 deposition cycles (e.g., Figures S10c,d, Supporting Information).

Surprisingly, in the case of $[Zn_4O(mipcapz)_3]_n$, only moderate crystallinity of the films was observed. The in situ monitored growth behavior (Figure S6, Supporting Information) reveals increased mass uptake during the exposure of the substrates to basic zinc acetate, as expected. Nevertheless, and in contrast to the other cases, almost all of the applied mipcapz linkers were removed during the washing step with ethanol, indicating poor nucleation and inefficient crystal growth of the methyl/isopropyl-substituted $[Zn_4O(mipcapz)_3]_n$ MOF. Accordingly, the obtained samples of $[Zn_4O(mipcapz)_3]_n$ reveal the lowest crystallinity (poor signal-to-noise ratio of the XRD peaks) among all of the deposited MOFs in this study. A highly efficient crystal growth stage after the prior nucleation stage is required to achieve excellent crystallinity of the MOF films.

2.1.2. MOF Film Adsorption Properties

Using an environmentally controlled QCM, the sorption properties of the homostructured MOF films were investigated. The methanol sorption isotherms at 25 °C exhibit the expected Langmuir type I shape without hysteresis, which illustrates the microporosity (**Figure** 4). The kinetic size of the methanol molecule is smaller than the pore opening windows for the entire series of $[ZnO(L)_3]_n$; therefore, the amount of methanol adsorbed at relative humidity, a P/P_0 of 0.95 (at 25 °C, 1 atm total pressure), is used to calculate the accessible pore volume of the synthesized MOF films (details are presented in Table S1, Supporting Information). In comparison to the films fabricated using the static stepwise deposition method in our previous report,[19] the new films obtained using the continuous step-by-step LPE method show methanol uptakes that are significantly increased by 7% to 55%. This observation is attributed to the much improved crystallinity of the new films (less amorphous components), especially in the cases of $[Zn_4O(mecapz)_3]_n$ and $[Zn_4O(mpcapz)_3]_n$. The increased bulkiness of the substituents at the carboxypyrazolate linkers in the series H_2dmcapz → H_2mecapz → H_2mpcapz results in the reduction of the saturation uptake and, therefore, the total pore volume. However, the dramatic decrease in the methanol total uptake observed in $[Zn_4O(mipcapz)_3]_n$ is explained by the much lower crystallinity of this particular film. Therefore, the effective pore volume derived for the homostructured $[Zn_4O(mipcapz)_3]_n$ film is not comparable with the expected value deduced from the respective, idealized MOF structure. The MOF film fabrication needs to be modified to achieve the expected adsorption capacity of the $[Zn_4O(mipcapz)_3]_n$ MOF film, which is discussed in Section 2.2.

Using slightly larger adsorbents than methanol with similar chemical functionality, such as ethanol and isopropanol, the effective pore window can be probed (Figure S12, Supporting Information). The highly crystalline films of dimethyl-substituted $[Zn_4O(dmcapz)_3]_n$ and methyl/ethyl-substituted $[Zn_4O(mecapz)_3]_n$ show almost the same adsorption amounts, indicating nearly equal pore openings of both MOFs, which also allow for the accommodation of isopropanol. Interestingly, after achieving a saturated loading of the methyl/propyl-substituted $[Zn_4O(mpcapz)_3]_n$, the isopropanol is hardly desorbed, as observed by the difference (hysteresis) between the adsorption and desorption isotherms. From this phenomenon, the effective

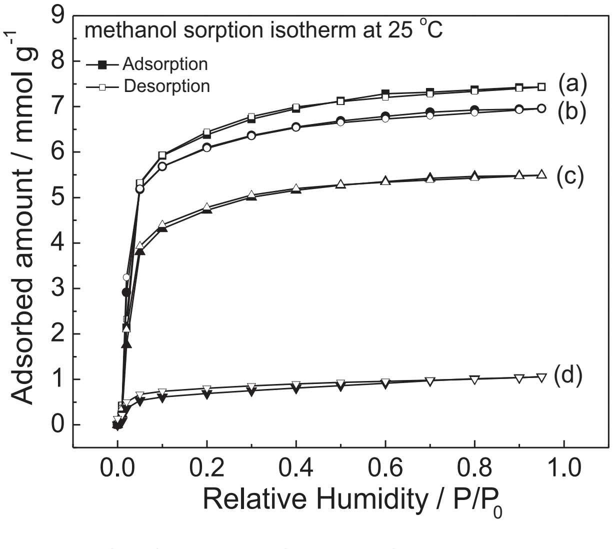

Figure 4. Methanol sorption isotherm at ambient temperature (25 °C) using an environmentally controlled quartz crystal microbalance (BEL-QCM-4 equipment) of homostructured MOF films of a) $[Zn_4O(dmcapz)_3]_n$, b) $[Zn_4O(mecapz)_3]_n$, c) $[Zn_4O(mpcapz)_3]_n$, and d) $[Zn_4O(mipcapz)_3]_n$ fabricated by the continuous step-by-step LPE deposition at 40 °C for 40 cycles on the –COOH functionalized QCM substrates.

pore window of [$Zn_4O(mpcapz)_3]_n$ was estimated to be approximately 5.1 Å, matching the kinetic size of isopropanol. We must note that the homostructured methyl/isopropyl-substituted [$Zn_4O(mipcapz)_3]_n$ film shows no uptake of isopropanol, which attracted our interest to fabricate this particular MOF film as a sorption selective layer, expressing the potential model for further separating applications (see Section 2.2, below). All of the MOF films, [$Zn_4O(mpcapz)_3]_n$ in particular, can be fully re-activated after the adsorption/desorption measurements by exchanging the adsorbed or remaining alcohol guests within the pore with methanol and then applying an in situ activation protocol at 70 °C for 2 h under dry Helium gas flow (quantitative desorption of methanol) before the next measurement.

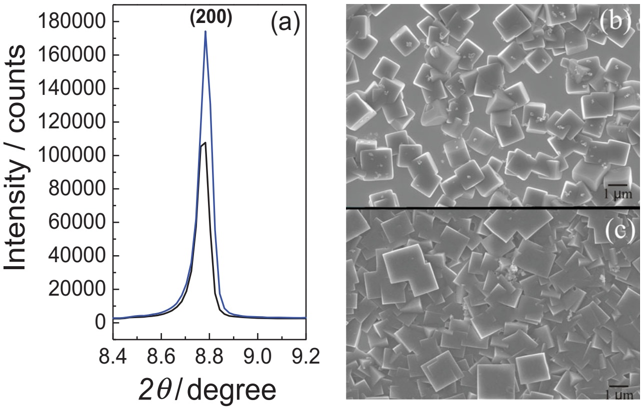

Figure 5. a) Intensity comparison at the (200) mirror plane of the XRD patterns of the homostructured [$Zn_4O(dmcapz)_3]_n$ 20 cycles (black) and the following heteroepitaxial [$Zn_4O(mpcapz)_3]_n$ 20 cycles on [$Zn_4O(dmcapz)_3]_n$ 20 cycles films (blue) fabricated by the continuous step-by-step LPE method at 40 °C on the –COOH functionalized QCM substrates; b,c) the corresponding SEM images.

2.2. Heteroepitaxial [$Zn_4O(L)_3]_n$ MOF-on-MOF Core–Shell Films B@A

2.2.1. MOF Film Growth

In the section above, we described that our attempts to achieve highly crystalline homostructured methyl/isopropyl-substituted [$Zn_4O(mipcapz)_3]_n$ films failed. To overcome this problem, the concept of heteroepitaxial growth via the continuous step-by-step LPE method of one MOF **B** on the surface of a previously deposited high crystalline seed MOF **A** was applied. As a model for separating membranes, the smallest pore opening [$Zn_4O(mipcapz)_3]_n$ was chosen as the particular MOF **B**, and it was fabricated on top of some larger pore opening MOF **A** to obtain the hybrid function of size exclusion absorption.[9d–f] Herein, [$Zn_4O(dmcapz)_3]_n$ or [$Zn_4O(mecapz)_3]_n$ was selected as the core MOF **A** component because of the favorable continuous LPE growth behavior, as described above, combined with the wider pore opening window in comparison to the other analogs. After 20 initial deposition cycles of the wide pore core component **A**, the narrow pore shell component **B** ([$Zn_4O(mecapz)_3]_n$, [$Zn_4O(mpcapz)_3]_n$ or [$Zn_4O(mipcapz)_3]_n$) was deposited on top of the pre-deposited **A** for an additional 20 cycles. This resulted in 40-cycle MOF B@A heterostructured films (similar overall thickness as the homostructured reference films of Section 2.1.) The XRD patterns of the heteroepitaxial [$Zn_4O(L)_3]_n$**B@A** films (Figure S13, Supporting Information) show a high signal-to-noise ratio, which indicates the high degree of crystallinity of the heterostructured MOF films. According to the same unit cell parameter of the two analogous MOF components **A** and **B**, a single phase is indexed in the XRD patterns, which agrees with the idea of lattice matching in the heteroepitaxial growth.

The increased (200) peak intensity of the **B@A** sample (20-cycle [$Zn_4O(mpcapz)_3]_n$ on top of 20-cycle [$Zn_4O(dmcapz)_3]_n$) compared to the respective 20-cycle film of the homostructured core component [$Zn_4O(dmcapz)_3]_n$ (**A**) indicates the successful formation of the desired **B@A** film (**Figure 5**a). An inspection of the SEM image of the core MOF **A** after 20 deposition cycles reveals the (expected) incomplete surface coverage of the seed crystals as a result of the island growth mode (Figure 5b). The subsequent heteroepitaxial growth (20 cycles) of the shell component **B** can occur at all facets of the seeding core crystals **A** as a consequence of the isotropic cubic lattice of the [$Zn_4O(L)_3]_n$ MOFs. Consequently, the seeding MOF **A** as a core is completely overgrown by the MOF **B** as a shell resulting in the increasing of the crystallite particle sizes, and eventually, the full surface coverage of the substrate is achieved (intergrown MOF **B** shell crystals; Figure 5c). Moreover, the orientation of the shell part **B** maintains the (100) preferable orientation of the MOF **A**. These results nicely emphasize the advantage of the continuous step-by-step LPE method in the fabrication of the hybridized **B@A** films consisting of some MOF component **B** (e.g., [$Zn_4O(mipcapz)_3]_n$), which is difficult (or even impossible) to deposit as phase-pure and highly crystalline homostructured component **A** (as discussed in Section 2.1.) In other words, certain nucleation problems of some MOF **B** on a given substrate can be overcome by selecting an appropriate seed MOF **A**. Interestingly, the total film growth rate observed by the in situ QCM monitoring (Figure S14, Supporting Information) of [$Zn_4O(mipcapz)_3]_n$ on the appropriate seed MOF **A** was increased roughly two-fold with respect to the homostructured (without seeding) deposition.

2.2.2. MOF Film Adsorption Properties

The sorption properties of the heterostructured **B@A** films were investigated on the QCM. In general, the sorption isotherms of alkanols match the expected Langmuir type I if the size of the adsorbed alkanol molecules is smaller than the pore opening window of the MOF. Interestingly, the specific alkanol adsorptions of these **B@A** MOF films do not fall between the properties of the respective homostructured core and shell MOFs, as observed in the cases of the corresponding heterostructured layer-pillar-type SURMOFs in our recent report.[21] Instead, the saturation amounts of the series of heterostructured **B@A** films are approximately equal to the saturation amount of the respective homostructured shell component MOF **B**, if this latter MOF film exhibits a very high crystallinity (**Figure 6**). For example, the saturation amount of methanol at the heteroepitaxial film **B@A**, that is, [$Zn_4O(mecapz)_3]_n$

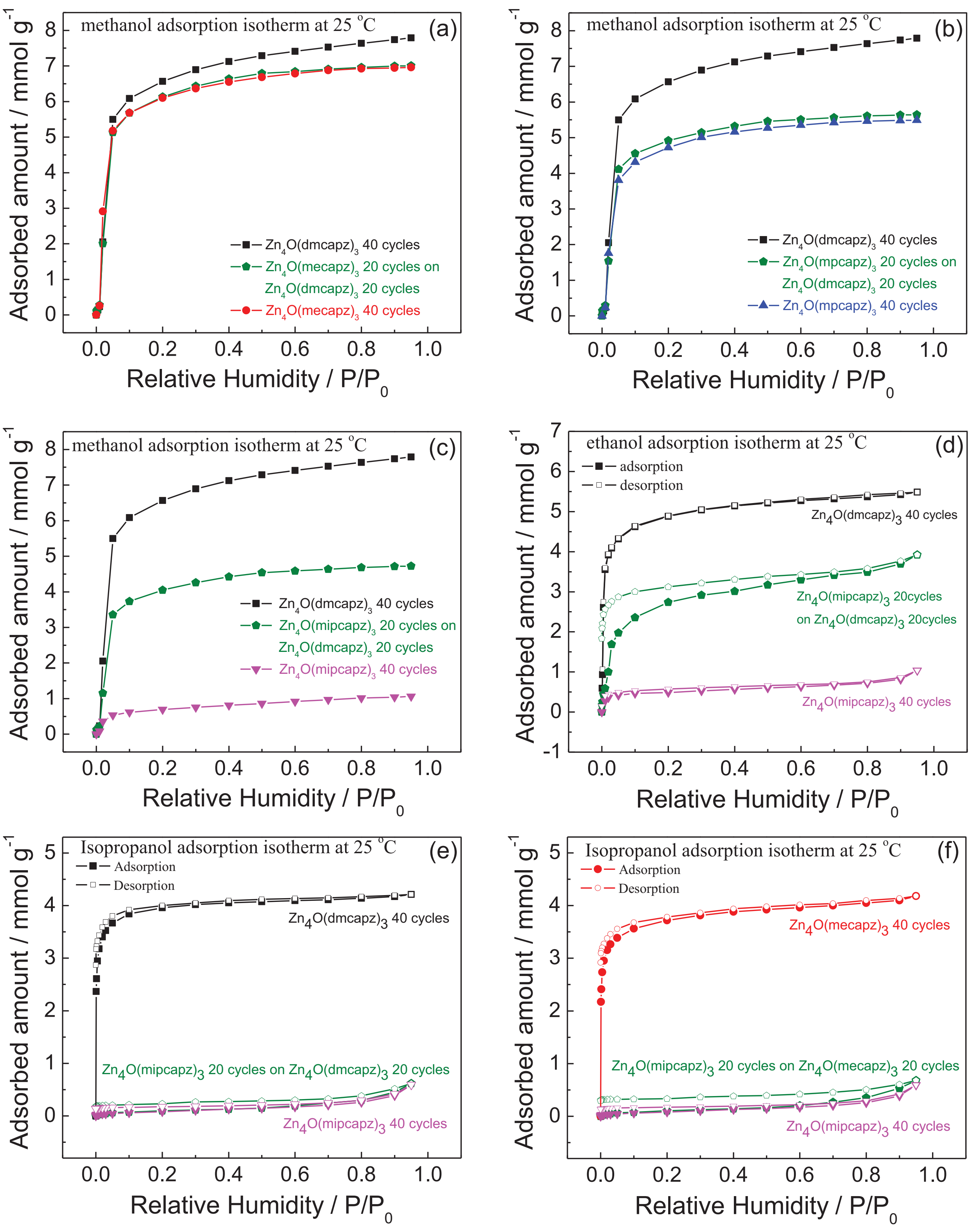

Figure 6. Methanol sorption isotherms at ambient temperature (25 °C) using an environmentally controlled QCM of the heteroepitaxial core-shell **B@A** MOF films of a) $[Zn_4O(mecapz)_3]_n$ 20 cycles on $[Zn_4O(dmcapz)_3]_n$ 20 cycles, b) $[Zn_4O(mpcapz)_3]_n$ 20 cycles on $[Zn_4O(dmcapz)_3]_n$ 20 cycles; c) methanol, d) ethanol, and e) isopropanol sorption isotherm of $[Zn_4O(mipcapz)_3]_n$ 20 cycles on $[Zn_4O(dmcapz)_3]_n$ 20 cycles, and f) isopropanol sorption isotherm of $[Zn_4O(mipcapz)_3]_n$ 20 cycles on $[Zn_4O(mecapz)_3]_n$ 20 cycles in comparison with the corresponding homostructured MOF films.

on $[Zn_4O(dmcapz)_3]_n$ (Figure 6a), and $[Zn_4O(mpcapz)_3]_n$ on $[Zn_4O(dmcapz)_3]_n$ (Figure 6b), are quite similar to the uptake of the highly crystalline homostructured films $[Zn_4O(mecapz)_3]_n$ and $[Zn_4O(mpcapz)_3]_n$, respectively (which were used as shell components **B**; other examples are shown in Figures S15,S16, Supporting Information). At present, we do not have additional evidence suitable for an explanation as to why the saturation uptakes of the **B@A** films are dominated by the property of the shell component. Nevertheless, the data clearly indicate the successful fabrication of a very high crystallinity MOF **B** by the heteroepitaxial growth on top of the existing crystalline seed MOF **A** in the core-shell fashion, but not as a mixing of separate crystals of the two components. Based on these results, the adsorption capacity of the $[Zn_4O(mipcapz)_3]_n$ MOF can instead be reasonably estimated using the adsorption capacity of the highly crystalline $[Zn_4O(mipcapz)_3]_n$ on $[Zn_4O(dmcapz)_3]_n$ hybrid **B@A** film. With the total adsorbed methanol amount of 4.726 mmol g^{-1} of the **B@A** film (Figure 6c), the accessible pore volume of $[Zn_4O(mipcapz)_3]_n$ can be calculated to be 0.241 cm^3 per cm^3 MOF, which is rational in comparison with the other homostructured MOF films, as mentioned above. Interestingly, the $[Zn_4O(mipcapz)_3]_n$ on $[Zn_4O(dmcapz)_3]_n$**B@A** film allows methanol and ethanol molecules (Figure 6c,d), but not isopropanol molecules (Figure 6e), to be adsorbed, indicating the molecular sieve function of the outer component $[Zn_4O(mipcapz)_3]_n$ when grown in high crystallinity. This result again emphasizes that the outer MOF component **B** is grown on top of the inner MOF component **A** in the core-shell fashion. In other words, core MOF **A** is nicely imbedded into a matrix of densely intergrown MOF **B** shell crystals without the presence of separate crystals **A** or **B** or **B@A** islands or platelets on the substrate surface. From the adsorption data, we conclude that the larger pore opening windows present in MOF film **A** are fully covered by the smaller pore opening windows of MOF film **B**. Only in such a case can one expect the proper function of the shell MOF **B** as the selective layer to allow size exclusion and only small enough probe molecules to be adsorbed inside the MOF films.

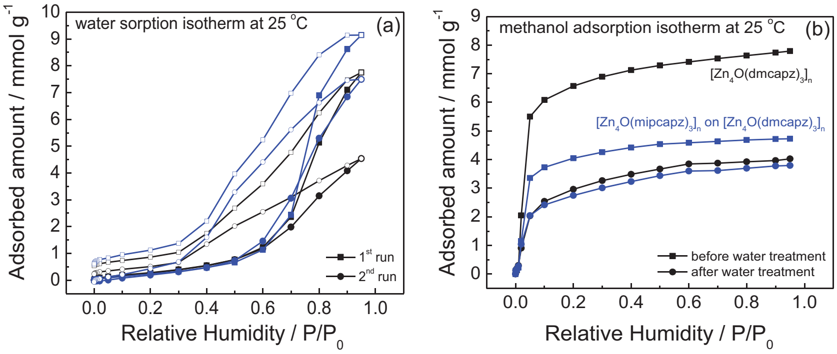

Figure 7. a) Water vapor sorption isotherm at 25 °C of the homostructured $[Zn_4O(dmcapz)_3]_n$ (black curves) and the heteroepitaxial $[Zn_4O(mipcapz)_3]_n$ on $[Zn_4O(dmcapz)_3]_n$ films (blue curves). The square and the circle symbols represent the first and the second run of water isotherms, respectively. The closed and open symbols indicate the adsorption and desorption measurements, respectively. b) Methanol sorption isotherm at 25 °C of the selected MOF films after two complete cycles of water vapor sorption isotherm treatments in comparison with the corresponding isotherms before water treatment.

2.3. Moisture Tolerance

For integration into practical devices, the stability of MOFs over moisture at ambient conditions is an important concern. The moisture tolerance of the fabricated MOF thin films was tested by performing a series of water vapor sorption isotherm measurements at 25 °C using the QCM instrument. The homostructured $[Zn_4O(dmcapz)_3]_n$ (**A**) and the heterostructured $[Zn_4O(mipcapz)_3]_n$ on $[Zn_4O(dmcapz)_3]_n$ (**B@A**) MOF films exhibit type III isotherms, indicating that water molecules are not adsorbed up to $P/P_0 = 0.6$ (60% relative humidity). However, multilayer condensation is observed when operating at higher relative humidity (**Figure 7**a). There are no significant differences in the crystallinity of the MOF films and methanol uptakes after two complete treatments with water vapor at 60% humidity, that is, adsorption/desorption cycles (Figure S18, Supporting Information). These results suggest the robustness of the films over moisture, which provides the possibility for applications at ambient conditions (relative humidity up to 60% at room temperature). However, after water treatment at a high humidity of 95%, the methanol uptake was reduced to approximately 48% of the total adsorbed amount observed for the reference homostructured $[Zn_4O(dmcapz)_3]_n$ **A** film (Figure 7b). This reduction in adsorption capacity can be explained by the gradual hydrolysis of the Zn–O coordinative bonds and, hence, by partial framework collapse. Interestingly, only 20% reduced adsorption capacity after water treatment at 95% humidity was observed in the case of the heteroepitaxial $[Zn_4O(mipcapz)_3]_n$ on $[Zn_4O(dmcapz)_3]_n$ **B@A** MOF film, showing the higher stability over moisture of $[Zn_4O(mipcapz)_3]_n$ than $[Zn_4O(dmcapz)_3]_n$. As more bulky alkyl substituents are located at the pyrazolate ring and point towards the labile Zn-O coordinative bonds, better protection against nucleophilic attacks of water can be observed. This finding again emphasizes the merits of fabricating the hybrid **B@A** MOF films.

3. Conclusions

The continuous step-by-step LPE technique provides an outstanding improvement in the crystallinity of the MOF-5 isotype carboxypyrazolato-type $[Zn_4O(L)_3]_n$ MOF thin films. The in-situ monitoring of the mass uptake during LPE growth by QCM serves as a guideline for control of the film growth, which strongly influences the observed crystallinity of the products. The schematic illustration (Scheme 1) describes the summarized messages of the fabrication of both the homostructured films **A** and the heteroepitaxial **B@A** films using the continuous step-by-step LPE method. $[Zn_4O(mipcapz)_3]_n$ films, which exhibit a moderate crystallinity when grown as a homostructured film **A**, can be deposited with very high crystallinity using the heteroepitaxial growth of this MOF as component **B** on top of the previously deposited highly crystalline component **A**. The outer component **B** begins to grow on all facets of the seeding component **A** until providing the fully covered core-shell heteroepitaxial films **B@A**. The heterostructured [Zn$_4$O(mipcapz)$_3$]$_n$ on [Zn$_4$O(dmcapz)$_3$]$_n$ film reveals hybrid functionality and exhibits good adsorption selectivity based on the size selection by the small pore opening window of the [Zn$_4$O(mipcapz)$_3$]$_n$ shell component, **B**. Therefore, methanol and ethanol are selectively adsorbed over isopropanol. Moreover, the adsorbed molecules can be stored with higher capacity within the **B@A** film as a result of the excellent crystallinity of components **B** and **A** compared to the poor crystallinity of the [Zn$_4$O(mipcapz)$_3$]$_n$ deposited as a single, homostructured film. This heterostructured MOF film could be one of the promising candidates for use in selective membrane applications because of its reasonable adsorption capacity, excellent size-selective adsorption of different alcohols and high degree of moisture-tolerance. Based on the lattice matching concept of the step-by-step heteroepitaxial growth, more complex structured multi-functionalized films could be achieved in this well-controlled manner, which open the path for specific applications.

4. Experimental Section

Materials: All starting materials were synthesized using the procedure reported in our previous work.[19] Basic zinc acetate [Zn$_4$O(CH$_3$COO)$_6$] was synthesized by the sublimation of zinc acetate dihydrate at 280 °C under vacuum.[22] The syntheses of 3-alkyl-5-alkyl-4-carboxypyrazole (H$_2$aacapz) functionalized linkers were performed according to the published method (see Supporting Information for details).[23]

Preparation of Homostructured [Zn$_4$O(L)$_3$]$_n$ MOF and Heterostructured B@A MOF Films: The gold-coated quartz crystal microbalance (QCM) substrates were functionalized to obtain the –COOH or –OH terminated surface by 16-mercaptohexadecanoic acid (MHDA) or 1-mercaptoundecanol (MUD) SAMs, respectively. The precursor solutions were prepared as follows: basic zinc acetate (1.0 mm) in technical grade ethanol and the carboxypyrazolate linkers (0.5 mm) in ethanol/water mixture (3:1 v/v). Typical continuous step-by-step LPE depositions of the MOF thin films were performed on the automated QCM instrument (Q-Sense E4 Auto) at 40 °C with a flow rate of 100 µL min^{-1}. In each cycle, the functionalized QCM substrate was successively exposed to the solution of basic zinc acetate (10 min), ethanol (washing step for 5 min), the linker (10 min) and ethanol (washing step for 5 min) as a continuous flow through the substrate surface. The homostructured [Zn$_4$O(L)$_3$]$_n$ MOF films were fabricated for 20 or 40 cycles. In the case of heterostructured B@A MOF films, 20 cycles of the smaller pore opening MOF B were fabricated on top of 20 cycles of the predeposited larger pore opening seed MOF A (i.e., [Zn$_4$O(mipcapz)$_3$]$_n$ on [Zn$_4$O(dmcapz)$_3$]$_n$). The in-situ growth of MOF films was monitored by the frequency change, which is related to the mass change, on the QCM substrate according to the Sauerbrey equation.[20]

Characterization: The crystalline phase of the MOF films were analyzed by powder X-ray diffraction (XRD) data collected on X'Pert PanAnalytical equipment (Bragg-Brentano geometry, Cu K radiation, 2θ from 5° to 50°, position sensitive detector). The crystal plane orientations were characterized via two-dimensional grazing incidence X-ray diffractions (2D-GIXRD) performing at Beamline 9 of DELTA (synchrotron X-ray wavelength of 1.00 Å, sample-to-detector distance of 391 cm and incidence angle of 0.1°). The morphology of the synthesized MOF films was examined using a scanning electron microscope (LEO 1530 Gemini).

Volatile Organic Compound Vapor Sorption Isotherm Measurements: The alkanol sorption isotherms of the obtained MOF films were studied using an environmentally controlled quartz crystal microbalance (BEL-QCM-4 equipment, BEL Japan) at 25 °C. Prior to the sorption measurements, the samples were activated by immersing in dichloromethane for 24 h (exchanging molecules within the pores) and the in situ activation was performed in a BEL-QCM instrument at 70 °C under dry helium gas flow (100 sccm) for 2 h until the frequency was stable (±5 Hz). The desired relative vapor pressure, P/P_0 (at 1 atm total pressure), of saturated organic vapor in helium gas was controlled in a range of 0.0–95.0% by three independent mass flow controllers. The specific adsorption amount was calculated from the observed QCM frequency using the Sauerbrey equation.

Supporting Information

Supporting Information is available from the Wiley Online Library or from the author.

Acknowledgements

This work was funded within the Priority Program 1362 “Metal-Organic Frameworks” of the German Research Foundation (DFG). DELTA is acknowledged for the grazing incidence X-ray diffraction measurements at BL09 (proposal number 01, first half of 2013). S.W. is grateful for Master and PhD scholarship from the Royal Thai Government under the Ministry of Science and Technology. M.T. is grateful for a PhD fellowship from the China Scholarship Council (CSC).

Received: August 14, 2013
Revised: October 29, 2013
Published online: December 20, 2013

---

[1] a) H. Li, M. Eddaoudi, M. O'Keeffe, O. M. Yaghi, *Nature* **1999**, *402*, 276; b) S. Kitakawa, R. Kitaura, S. Noro, *Angew. Chem.* **2004**, *116*, 2388; *Angew. Chem. Int. Ed.* **2004**, *43*, 2334; c) G. Férey, C. Mellot-Draznieks, C. Serre, F. Millange, *Acc. Chem. Res.* **2005**, *38*, 217; d) S. R. Batten, R. Robson, *Angew. Chem.* **1998**, *110*, 1558; *Angew. Chem. Int. Ed.* **1998**, *37*, 1460.

[2] a) M. Dincă, A. Dailly, Y. Liu, C. M. Brown, D. A. Neumann, J. R. Long, *J. Am. Chem. Soc.* **2006**, *128*, 16876; b) M. Dincă, J. R. Long, *Angew. Chem. Int. Ed.* **2008**, 47, 6766; c) R. Matsuda, R. Kitaura, S. Kitagawa, Y. Kubota, R. V. Belosludov, T. C. Kobayashi, H. Sakamoto, T. Chiba, M. Takata, Y. Kawazoe, Y. Mita, *Nature* **2005**, *436*, 238; d) L. J. Murray, M. Dincă, J. R. Long, *Chem. Soc. Rev.* **2009**, *38*, 1294.

[3] a) B. Wang, A. P. Côté, H. Furukawa, M. O'Keeffe, O. M. Yaghi, *Nature*, **2008**, *453*, 207; b) J.-R. Li, R. J. Kuppler, H.-C. Zhou, *Chem. Soc. Rev.* **2009**, *38*, 1477.

[4] a) J. S. Seo, D. Whang, H. Lee, S. I. Jun, J. Oh, Y. J. Jeon, K. Kim, *Nature*, **2000**, *404*, 982; b) C.-D. Wu, A. Hu, L. Zhang, W. Lin, *J. Am. Chem. Soc.* **2005**, *127*, 8940; c) J. Y. Lee, O. K. Farha, J. Roberts, K. A. Scheidt, S. T. Nguyen, J. T. Hupp, *Chem. Soc. Rev.* **2009**, *38*, 1450.

[5] a) M. D. Allendorf, R. J. T. Houk, L. Andruszkiewicz, A. A. Talin, J. Pikarsky, A. Choudhury, K. A. Gall, P. J. Hesketh, *J. Am. Chem. Soc.* **2008**, *130*, 14404; b) L. E. Kreno, K. Leong, O. K. Farha, M. Allendorf, R. P. Van Duyne, J. T. Hupp, *Chem. Rev.* **2011**, *112*, 1105.

[6] P. Horcajada, T. Chalati, C. Serre, B. Gillet, C. Sebrie, T. Baati, J. F. Eubank, D. Heurtaux, P. Clayette, C. Kreuz, J.-S. Chang, Y. K. Hwang, V. Marsaud, P.-N. Bories, L. Cynober, S. Gil, G. Férey, P. Couvreur, R. Gref, *Nat. Mater.* **2010**, *9*, 172.

[7] M. Eddaoudi, J. Kim, N. Rosi, D. Vodak, J. Wachter, M. O'Keeffe, O.M. Yaghi, *Science* **2002**, *295*, 469.

[8] a) Z. Wang, S. M. Cohen, *J. Am. Chem. Soc.* **2007**, *129*, 12368; b) Z. Q. Wang, S. M. Cohen, *Angew. Chem.* **2008**, *120*, 4777; *Angew. Chem. Int. Ed.* **2008**, *47*, 4699; c) S. M. Cohen, *Chem. Rev.* **2012**, *112*, 970.

[9] a) S. Furukawa, K. Hirai, K. Nakagawa, Y. Takashima, R. Matsuda, T. Tsuruoka, M. Kondo, R. Haruki, D. Tanaka, H. Sakamoto, S. Shimomura, O. Sakata, S. Kitakawa, *Angew. Chem. Int. Ed.* **2009**, *48*, 1766; b) K. Koh, A. G. Wong-Foy, A. J. Matzger, *Chem. Commun.* **2009**, 6162; c) S. Furukawa, K. Hirai, Y. Takashima, K. Nakagawa, M. Kondo, T. Tsuruoka, O. Sakata, S. Kitakawa, *Chem. Commun.* **2009**, 5097; d) K. Hirai, S. Furukawa, M. Kondo, H. Uehara, O. Sakata, S. Kitakawa, *Angew. Chem. Int. Ed.* **2011**, *50*, 8057; e) K. Hirai, S. Furukawa, M. Kondo, M. Meilikhov, Y. Sakata, O. Sakata, S. Kitakawa, *Chem. Commun.* **2012**, *48*, 6472; f) K. Hirai, K. Chen, T. Fukushima, S. Horike, M. Kondo, N. Louvain, C. Kim, Y. Sakata, M. Meilikhov, O. Sakata, S. Kitakawa, S. Furukawa, *Dalton Trans.* **2013**, *42*,15868.

[10] a) D. Zacher, O. Shekhah, C. Wöll, R. A. Fischer, *Chem. Soc. Rev.* **2009**, *38*, 1418; b) A. Bétard, R. A. Fischer, *Chem. Rev.* **2012**, *112*, 1055; c) O. Shekhah, J. Liu, R. A. Fischer, C. Wöll, *Chem. Soc. Rev.* **2011**, *40*, 1081.

[11] a) M. D. Allendorf, R. J. T. Houk, L. Andruszkiewicz, A. A. Talin, J. Pikarsky, A. Choudhury, K. A. Gall, P. J. Hesketh, *J. Am. Chem. Soc. 2008*, *130*, 14404; b) G. Lu, J. T. Hupp, *J. Am. Chem. Soc.* **2010**, *132*, 7832.

[12] a) J. Gascon, F. Kapteijn, *Angew. Chem. Int. Ed.* **2010**, *49*, 1530; b) A. Bétard, H. Bux, S. Henke, D. Zacher, J. Caro, R. A. Fischer, *Microporous Mesoporous Mater.* **2012**, *150*, 76.

[13] A. S. Münch, J. Seidel, A. Obst, E. Weber, F. O. R. L. Mertens, *Chem. Eur. J.* **2011**, *17*, 10958.

[14] B. Liu, M. Ma, D. Zacher, A. Bétard, K. Yusenko, N. Metzler-Nolte, C. Wöll, R. A. Fischer, *J. Am. Chem. Soc.* **2011**, *133*, 1734.

[15] a) O. Shekhah, H. Wang, D. Zacher, R. A. Fischer, C. Wöll, *Angew. Chem. Int. Ed.* **2009**, *48*, 5038; b) D. Zacher, R. Schmid, C. Wöll, R. A. Fischer, *Angew. Chem. Int. Ed.* **2011**, *50*, 176.

[16] a) O. Shekhah, K. Hirai, H. Wang, H. Uehara, M. Kondo, S. Diring, D. Zacher, R. A. Fischer, O. Sakata, S. Kitakawa, S. Furukawa, C. Wöll, *Dalton Trans.* **2011**, *40*, 4954; b) D. Zacher, K. Yusenko, A. Bétard, S. Henke, M. Molon, T. Ladnorg, O. Shekhah, B. Schüpbach, T. de los Arcos, M. Krasnopolski, M. Meilikhov, J. Winter, A. Terfort, C. Wöll, R. A. Fischer, *Chem. Eur. J.* **2011**, *17*, 1448; c) B. Liu, M. Tu, D. Zacher, R. A. Fischer, *Adv. Funct. Mater.* **2013**, *23*, 3790; d) M. Meilikhov, S. Furukawa, K. Hirai, R. A. Fischer, S. Kitakawa, *Angew. Chem.* **2013**, *125*, 359.

[17] a) O. Zybaylo, O. Shekhah, H. Wang, M. Tafipolsky, R. Schmid, D. Johannsmann, C. Wöll, *Phys. Chem. Chem. Phys.* **2010**, *12*, 8092; b) V. Stavila, J. Volponi, A. M. Katzenmeyer, M. C. Dixon, M. D. Allendorf, *Chem. Sci.* **2012**, *3*, 1531.

[18] C. Montoro, F. Linares, E. Q. Procopio, I. Senkovska, S. Kaskel, S. Galli, N. Masciocchi, E. Barea, J. A. R. Navarro, *J. Am. Chem. Soc.* **2011**, *133*, 11888.

[19] A. Bétard, S. Wannapaiboon, R. A. Fischer, *Chem. Commun.* **2012**, *48*, 10493.

[20] a) G. Sauerbrey, *Z. Phys.* **1959**, *155*, 206; b) H. Uehara, S. Diring, S. Furukawa, Z. Kalay, M. Tsotsalas, M. Nakahama, K. Hirai, M. Kondo, O. Sakata, S. Kitakawa, *J. Am. Chem. Soc.* **2011**, *133*, 11932.

[21] M. Tu, S. Wannapaiboon, R. A. Fischer, *Dalton Trans.* **2013**, *42*,16029.

[22] S. Hausdorf, F. Baitalow, T. Böhle, D. Rafaja, F. O. R. L. Mertens, *J. Am. Chem. Soc.* **2010**, *132*, 10978.

[23] M. W. Rathke, P. J. Cowan, *J. Org. Chem.* **1985**, *50*, 2622.